Single-Shot Coherent Diffraction Imaging of Microbunched Relativistic Electron Beams for Free-Electron Laser Applications

A. Marinelli, M. Dunning, S. Weathersby, E. Hemsing, D. Xiang, G. Andonian, F. O'Shea, Jianwei Miao, C. Hast, and J. B. Rosenzweig

Phys. Rev. Lett. **110**, 094802 — Published 1 March 2013

DOI: 10.1103/PhysRevLett.110.094802

Single-shot coherent diffraction imaging of microbunched relativistic electron beams for free-electron laser applications

A. Marinelli,[1] M. Dunning,[2] S. Weathersby,[2] E. Hemsing,[2] D. Xiang,[2] G. Andonian,[1] F. O'Shea,[1] Jianwei Miao,[1] C. Hast,[2] and J. B. Rosenzweig[1]

[1]*Department of Physics and Astronomy, University of California Los Angeles, Los Angeles, CA 90095, USA*
[2]*SLAC National Accelerator Laboratory, Menlo Park, California 94025, USA*

With the advent of coherent X-rays provided by the X-ray free-electron laser (FEL), strong interest has been kindled in sophisticated diffraction imaging techniques. In this paper, we exploit such techniques for the diagnosis of the density distribution of the intense electron beams typically utilized in an X-ray FEL itself. We have implemented this method by analyzing the far-field coherent transition radiation emitted by an inverse-FEL microbunched electron beam. This analysis utilizes an oversampling phase retrieval method on the transition radiation angular spectrum to reconstruct the transverse spatial distribution of the electron beam. This application of diffraction imaging represents a significant advance in electron beam physics, having critical applications to the diagnosis of high-brightness beams, as well as the collective microbunching instabilities afflicting these systems.

X-ray free-electron lasers (XFELs) [1, 2] are a unique tool for the investigation of ultra-small and ultra-fast systems, permitting unprecedented studies of atomic-molecular structure at the angstrom length and femtosecond time scale. The XFEL is an example of a new class of intense, coherent electromagnetic sources, which can be fully exploited in measurements by the introduction of innovative, diffraction imaging-based techniques [3, 4]. Diffraction imaging requires the use of sophisticated phase-retrieval methods that indeed permit detailed investigations of spatial structures down to the X-ray diffraction limit. This new approach to imaging, stimulated by the burgeoning availability of coherent sources, is rapidly diffusing into a wide range of different applications. In this vein, we extend diffraction imaging techniques to a new frontier application in the physics of intense electron beams and provide a first demonstration of the newly proposed method.

An XFEL is a complex system that may be described as a controlled beam-radiation instability. The successful operation of an XFEL requires use of a low-emittance, high peak current electron beam. The generation, compression, and transport of such high-brightness relativistic electron beams poses many challenges, due particularly to parasitic beam instabilities that amplify the beam's shot-noise-derived microbunching during beam compression. This type of collective effect may be broadly identified as the microbunching instability (MBI) [5–9]. The MBI may generate strong perturbations in the beam's longitudinal phase-space which serve to reduce the efficiency of the downstream FEL [6, 10]. Most importantly, MBI may also induce the emission of coherent optical transition radiation (coherent OTR, or COTR) in beam diagnostics [11–14], severely compromising the utility of optical transition radiation-based measurements. While the effect of the microbunching instability on the FEL performance per se can be mitigated using a laser heater [10], this approach does not effectively suppress COTR emission in diagnostics [10]. This situation renders conventional OTR-based diagnostics ineffective for compressed high-brightness electron beams.

In this paper, utilizing methods originally employed in coherent X-ray imaging, we propose and experimentally test a method that exploits the coherent radiation rather than attempting to avoid or eliminate coherence effects in beam diagnostics. This approach, which uses the microbunching present in an electron beam to give a single-shot, far-field COTR image, yields a robust path for the reconstruction of the transverse spatial structure of the beam microbunching. We report on the experimental demonstration of this technique at the Next Linear Collider Test Accelerator (NLCTA), located at the SLAC National Accelerator Laboratory.

The coherent imaging technique proposed provides a general method for the reconstruction of the beam microbunching profile from the far-field COTR image. This technique has a number of important applications that depend on how the microbunching arises in the electron beam. For example, it can be applied as an advanced diagnostic for the FEL interaction, in which the entire electron beam transverse profile contributes to the formation of microbunching. It can also be applied to yet more complex cases, as typified by the space-charge induced optical microbunching, in which the beam density modulation may be transversely incoherent [8, 9], or to novel types of microbunching with more complex topological dependencies. An example of the latter case is found in the helical microbunching structure used to drive the emission of orbital angular momentum modes in FELs [15–17]. In this paper we will focus on a seeded scenario, in which the microbunching is generated uniformly across the transverse beam profile by the interaction of the beam with an external laser in a magnetic undulator. This represents a specific type of the inverse FEL interaction, here referred to as laser-induced microbunching (LIM). This case is particularly convenient, since, with

the laser turned off, it allows straightforward benchmarking of our coherent imaging technique with the incoherent OTR image of the beam's transverse profile. In this regard, it should be noted that reconstruction of the beam profile from LIM demonstrated here can be used to determine compressed beam distributions even in the presence of the MBI, as the LIM-derived coherent signal can easily be made to dominate over that due to the MBI. This provides an alternative solution to the mitigation of COTR in FEL injector diagnostics (see also [18] and [19]). In fact, the LIM may generally provide a direct map of the three-dimensional beam density distribution. A similar approach has also been proposed in a related context: the reconstruction of the beam's longitudinal profile, in a scheme known as an optical replica synthesizer [20]. In contrast, we will refer to the transverse reconstruction technique introduced here as the transverse optical replica (TOR). We note the attractive possibility that combining the two techniques would allow the single shot reconstruction of the three-dimensional electron beam structure [21]. It's also worth pointing out that the combination of the TOR technique with ultrashort seed laser pulses would allow the time resolved determination of the transverse distribution of the electron beam at the few femtosecond time-scale. Finally, we note that the TOR measurement could also be extended to cases in which no external seed is available such as the MBI. Generally the microbunching induced by the MBI is transversely incoherent [11], which means that the reconstruction of microbunching does not reproduce the beam's transverse profile. However, the effect of transverse Landau damping induced by emittance [8, 9] can be exploited through e-beam transport to induce transversely uniform microbunching to be used as a map of the density distribution. In this scenario, the TOR reconstruction technique captures only the fraction of the electron bunch that contributes to the coherent emission, which is typically the part of the bunch that lies close to the current peak.

The emission of coherent radiation from a relativistic electron beam requires the formation of a density modulation on the scale of the radiation wavelength. The beam density modulation can be described by the 3D bunching factor, defined as:

$$\tilde{b}(x,y,k_z) = \frac{1}{N}\int dz\rho(x,y,z)e^{-ikz_z}, \qquad (1)$$

where z is the longitudinal position along the beam axis, x, y are the transverse positions, $\rho(x,y,z)$ is the three-dimensional beam density distribution, N is the number of electrons in the beam and z_n is the longitudinal position of the n_{th} electron. Note that $\tilde{b}$ is a three-dimensional extension of the one-dimensional bunching factor commonly used in free-electron laser theory [22].

The experimental goal we are pursuing here is to reconstruct the spatial dependence of $\tilde{b}(x,y,k_z)$ from a single-shot COTR image by analyzing the beam's coherent emission characteristics. Near-field imaging of COTR yields a complex pattern given by the convolution of $\tilde{b}$ with the OTR near-field Green's function [21], which differs drastically from the transverse distribution of $\tilde{b}$ (for example, the near-field COTR image of an axisymmetric microbunched beam has a ring-like structure [13]). This means that direct near-field imaging of a microbunched beam profile is not possible, even in the case of uniform microbunching. Far-field imaging yields a more direct path to unfold the microbunching transverse structure from the coherent radiation pattern. To understand this approach, we first introduce the far-field COTR differential power spectrum emitted by a microbunched beam, defined as the energy radiated per unit frequency and unit solid angle [23]

$$\frac{dP}{d\omega d\Omega} = \frac{dP}{d\omega d\Omega}|_{sp} N^2 |B(k_x,k_y,k_z)|^2, \qquad (2)$$

where $\frac{dP}{d\omega d\Omega}|_{sp} = \frac{e^2}{4c\epsilon_0\pi^3}\frac{\beta^2\sin^2\theta}{(1-\beta^2\cos^2\theta)^2}$ indicates the single particle differential radiation spectrum, e is the electron charge, c is the speed of light, ϵ_0 is the vacuum permittivity and β is the beam velocity normalized to the speed of light. The polar angle is related to k_x, k_y, k_z by $\cos\theta = \frac{\sqrt{k_x^2+k_y^2}}{\sqrt{k_x^2+k_y^2+k_z^2}}$. The form factor B, or beam diffraction pattern, is defined as the 3D Fourier transform of the beam's charge density distribution:

$$B(k_x,k_y,k_z) = \frac{1}{N}\int dxdydz\ \rho(x,y,z)e^{-ik_x x - ik_y y - ik_z z}. \qquad (3)$$

$\tilde{b}(x,y,k_z)$ and $B(k_x,k_y,k_z)$ are a two-dimensional Fourier transform pair, *i.e.*

$$B(k_x,k_y,k_z) = \int dxdy\ \tilde{b}(x,y,k_z)e^{-ik_x x - ik_y y}. \qquad (4)$$

From the above definitions, it follows that, from a far-field COTR image one can measure the amplitude of B. The spatial dependence of the beam microbunching can be recovered by an inverse discrete Fourier transform (DFT). However, to invert the DFT one must also have information about the complex phase of B, which cannot be inferred directly from the far-field image. It has been recently understood that the phase of a 2D signal can be recovered by means of an iterative phase-retrieval algorithm, provided that $|B(k_x,k_y,k_z)|$ is sampled with high enough resolution in the frequency domain. The criterion that needs to be satisfied is $dk = 2\pi/OL_s$ [24] where dk is the resolution in the transverse frequency domain, L_s is the characteristic size of the beam in the space-domain and $O > \sqrt{2}$ is the oversampling ratio. In practice, L_s is chosen as the size of a finite support in x, y that fully contains the signal. This criterion is often referred to as

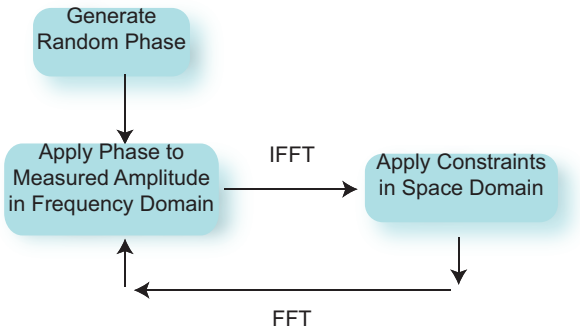

FIG. 1: Schematics of a phase-retrieval algorithm

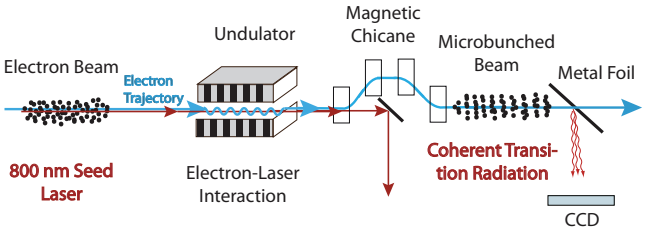

FIG. 2: Layout of the experimental setup.

the oversampling condition.

Iterative phase-retrieval algorithms (see e.g. [24, 25]) are now used in a great number of advanced applications, such as coherent diffraction imaging of non-crystalline samples [26]. Figure 1 shows a schematic of the algorithm, which begins by application of a random phase to the signal in the frequency domain. An inverse fast Fourier transform (IFFT) is then applied to obtain a trial signal in the spatial domain. At this point a given set of constraints (discussed below) is applied in the spatial-domain and a fast Fourier transform (FFT) is performed. Finally, one substitutes the amplitude in the frequency domain with the measured amplitude, while keeping the phase from the FFT. This process is repeated for multiple iterations (typically a few hundreds to thousands) until the amplitude of the final FFT is equal to the measured amplitude within a small tolerance.

The constraints applied in the spatial domain depend on the type of measurement performed but usually include a support constraint, i.e. the signal in x, y is constrained to vanish outside a given finite support [25]. Furthermore, if the beam microbunching is real and positive in the spatial-domain, a positivity constraint can be applied by keeping just the real part of the spatial-domain signal and setting to zero all data points having a negative value. The positivity constraint increases the speed of the reconstruction algorithm and ensures the uniqueness of the solution [25]. This constraint can be applied in the case of LIM induced by a laser that is larger than the transverse size of the beam, which is the physical scenario of interest in this paper. In this case, it can be shown that the microbunching distribution is $\tilde{b} \propto \int dz \rho(x, y, z)$ [21], which is an everywhere positive function that represents the transverse profile of the electron bunch.

To test the proposed method, we have performed a LIM-seeded COTR experiment at the NLCTA. The experimental schematic is shown in Fig.2. It corresponds to the first part of the ECHO beamline, which has been used for echo-enabled harmonics experiments in recent years [27, 28]. An electron beam of energy $E = 120$ MeV is sent through an undulator, co-propagating with a resonant laser of wavelength $\lambda = 800nm$. The resonant interaction generates an energy modulation in the electron beam which is then transformed into density modulation by a subsequent magnetic chicane. The electron beam is finally directed through a metal foil, causing emission of a COTR pulse that is detected by a CCD camera. The far-field pattern is collected with a commercial Navitar compound lens focused to infinity. A bandpass filter with a bandwidth of $10nm$ is used to eliminate the higher harmonics of the COTR pulse. The seed laser transverse size significantly exceeds that of the electron beam, giving a nearly transversely uniform electric field that interacts with the beam electrons. Thus the microbunching is, to an excellent approximation, a replica of the transverse shape of the electron beam. Since in the experiment we used an uncompressed beam which is not notably affected by the MBI, the coherent measurement can be benchmarked by comparison with a near-field incoherent OTR image obtained with no LIM applied, obtained by focusing the CCD camera on the OTR screen.

Figure 3 shows a far-field COTR image and the inferred beam form factor. Since the COTR single particle differential intensity is zero on axis, B cannot be measured for $k_x \simeq 0, k_y \simeq 0$. The amplitude of B close to the axis is then reconstructed by the retrieval algorithm simply keeping the amplitude and phase of the IFFT near the axis as the last step of each iteration. This issue is analogously found in coherent diffraction imaging experiments with X-rays, where the near-axis diffraction pattern is dominated by the direct beam (see e.g. Ref. [26]) and is commonly referred to as the missing center problem. Note also that Fig. 3 shows a slight asymmetry in the far-field pattern. This is due to residual dispersion in the bunching chicane and to fluctuations in the orbit of the electrons, which generate a slight tilt of the microbunching with respect to the z-axis (see e.g. Ref. [8]). This issue can be solved by shifting the far-field pattern so that the center of mass of the form factor lies on the $k_x = 0, k_y = 0$ point. Finally we note that the two-peak structure shown in Fig. 3 results from the vertical beam distribution shown in Fig. 4, which gives a horizontal form factor and, thus, a two-lobed far-field radiation pat-

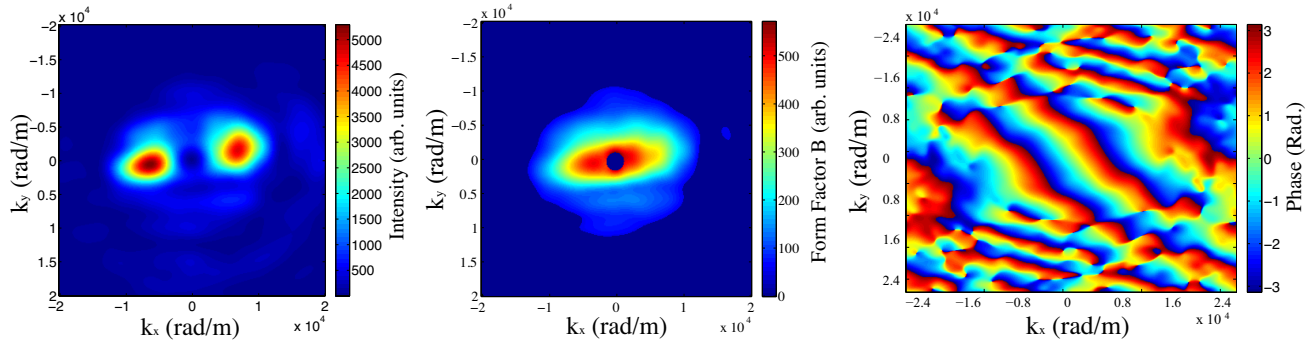

FIG. 3: Raw far-field COTR image (left image), inferred amplitude of the beam's form factor (center image), and reconstructed phase in the frequency domain (right image).

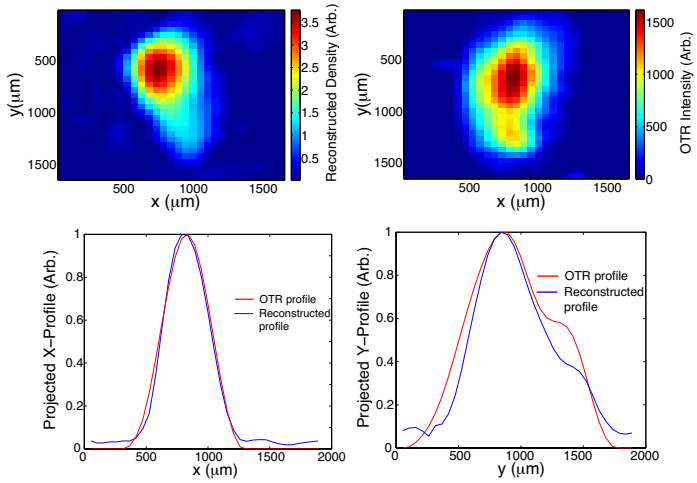

FIG. 4: Reconstructed microbunching in the space-domain from the diffraction pattern in Fig.3 (upper left image). For comparison an incoherent OTR image is shown (the upper right image). The bottom images show the x and y projected profiles of both images.

tern. The right plot on Fig. 3 shows the reconstructed phase of B. Figure 4 shows the resulting transverse dependence of the beam microbunching $\tilde{b}(x, y, k_z)$ and an incoherent OTR image of the beam. For ease of comparison the x and y projections of the reconstructed and measured beam distribution are shown. The relative error ϵ in the reconstructed image is defined as the absolute value of the difference between the measured and reconstructed form factors, integrated over the far-field plane, normalized to the integrated amplitude of the measured form factor. The error tolerance of the reconstruction was set to $\epsilon < 10^{-5}$.

The NLCTA beam possesses small shot-to-shot fluctuations of the beam transverse shape, which gives some slight variations in the comparison beam profiles, permitting a benchmarking of the measurement limited to the fluctuation levels. Even considering this limitation, there are numerous repeatable features of the beam profile that support comparison. The root mean square (RMS) sizes for the reconstructed and OTR profiles, averaged over 20 shots, are respectively $\sigma_{x,rec} \simeq (197 \pm 17)\mu m$ and $\sigma_{x,OTR} \simeq (201 \pm 11)\mu m$ for the horizontal axis and $\sigma_{y,rec} \simeq (317 \pm 28)\mu m$ and $\sigma_{y,OTR} \simeq (308 \pm 18)\mu m$ for the vertical axis. Finally, Fig. 5 shows the use of the reconstruction technique for a different beamline configuration, yielding a horizontal beam distribution. In this case the RMS sizes for the reconstructed and OTR profiles, averaged over 20 shots, are respectively $\sigma_{x,rec} \simeq (334 \pm 48)\mu m$ and $\sigma_{x,OTR} \simeq (343 \pm 33)\mu m$ for the horizontal axis and $\sigma_{y,rec} \simeq (172 \pm 52)\mu m$ and $\sigma_{y,OTR} \simeq (167 \pm 49)\mu m$ for the vertical axis. The two methods yield consistent results well within the fluctuations level, providing a benchmarking to the newly introduced coherent imaging approach. The rms variance in the measurement is mostly due to shot to shot beam size fluctuations and is not inherent to the measurement technique. The spatial resolution of the coherent diffraction imaging method is determined by the inverse of the highest spatial frequency effectively measured in the far-field image, which depends on several factors such as the electron beam size at the OTR screen, the CCD dynamic range, and the angular aperture of the collection optics. In general, the design of the experimental setup has to balance the need for strong oversampling, which requires the far-field image to occupy a large number of pixels, with the push for high resolution, which requires high intensity per pixel (so that the high spatial frequency components of the signal be well above the instrumental noise). In the measurements reported, the resolution is estimated to be approximately one fourth of the rms beam size.

In conclusion, in this Letter we have introduced, and experimentally tested, a new diffraction imaging-based technique for the single-shot reconstruction of the transverse shape of beam microbunching for a relativistic elec-

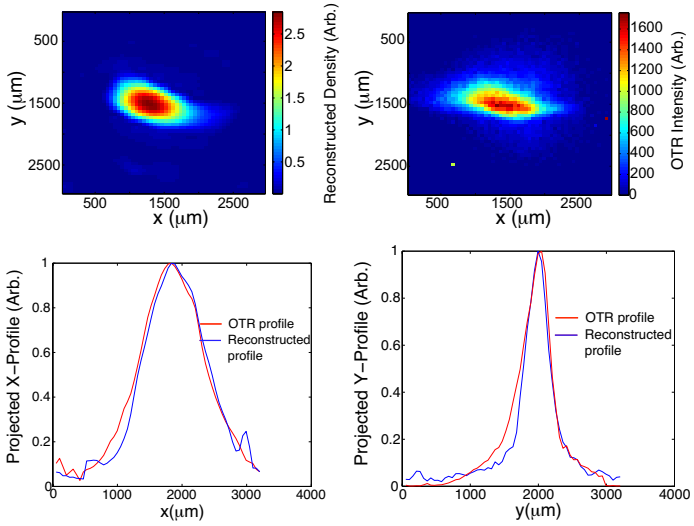

FIG. 5: Reconstructed microbunching (upper left image) and near field OTR image (upper right image) for a beamline configuration yielding a horizontal beam. The bottom images show the x and y projected profiles of both images.

tron beam. This technique is based on far-field COTR imaging and on application of a phase-retrieval algorithm. We have demonstrated this method for the case of laser-induced microbunching, in a seeded COTR experiment. This technique is generally applicable, and may be extended to measure arbitrary microbunching structures. The case of laser induced microbunching is of relevance to current and future XFELs since it extends the OTR-based profile measurements to compressed beams, even in the presence of COTR induced by the MBI. Further, we note that by combining this measurement to those discussed in [20], one may obtain a 3D replica of the beam distribution. Finally, in the absence of externally imposed microbunching, the method promises to be a keen tool in unfolding the details of the transverse spatial distribution of the collective instability-induced microbunching itself.

ACKNOWLEDGEMENTS

The authors would like to acknowledge C.C. Chen for his help with the coding of the phase-retrieval algorithm. This research is supported by grants from US DOE Contract Nos. DE-FG02-07ER46272 and DE-FG03-92ER40693, Office of Naval Research Contract No. N00014-06-1-0925, DARPA Contract No. N66001-11-4197 and DOE Contract No. DE-AC02-76SF00515.

[1] P. Emma, R. Akre, J. Arthur, R. Bionta, C. Bostedt, et al., Nat. Photon. **4**, 641 (2010).
[2] W. Ackermann G. Asova, V. Ayvazyan, A. Azima, N. Baboi, et al., Nat. Photon. **1**, 336 (2007).
[3] S. Boutet, L. Lomb, G. J. Williams, T. R. M. Barends, A. Aquila, et al., Science **337**, **6092**, 362-364(2012).
[4] H. N. Chapman , A. Barty, M. J. Bogan, S. Boutet, M. Frank, et al., Nat. Phys. **2**, 839 (2006).
[5] M. Borland, Y. Chae, P. Emma, J. Lewellen, V. Bharadwaj, et al., Nucl. Instrum. Methods Phys. Res., Sect. A **483**, 268 (2002), ISSN 0168-9002.
[6] Z. Huang, M. Borland, P. Emma, J. Wu, C. Limborg, et al. Phys. Rev. ST Accel. Beams **7**, 074401 (2004).
[7] G. Stupakov and S. Heifets, Phys. Rev. ST Accel. Beams **5**, 054402 (2002).
[8] D. Ratner, A. Chao, and Z. Huang, Proceedings of the 2008 Free-Electron Laser Conference p. 338 (2008).
[9] A. Marinelli and J. B. Rosenzweig, Phys. Rev. ST Accel. Beams **13**, 110703 (2010).
[10] Z. Huang, A. Brachmann, F.-J. Decker, Y. Ding, D. Dowell, et al., Phys. Rev. ST Accel. Beams **13**, 020703 (2010).
[11] A. H. Lumpkin, Y. C. Chae, J. W. Lewellen, W. J. Berg, M. Borland, et al., Nucl. Instrum. Meth. A **507**, 200 (2003).
[12] A. H. Lumpkin, N. S. Sereno, W. J. Berg, M. Borland, Y. Li, et al. Phys. Rev. ST Accel. Beams **12**, 080702 (2009).
[13] H. Loos and et al., Proceedings of the 2008 Free-Electron Laser Conference, Gyeongju, Korea p. 485. (2008).
[14] S. Wesch and et al., Proceedings of the 2009 Free-Electron Laser Conference, Liverpool, UK p. 619 (2009).
[15] E. Hemsing, P. Musumeci, S. Reiche, R. Tikhoplav, A. Marinelli, et al., Phys. Rev. Lett. **102**, 174801 (2009).
[16] E. Hemsing, A. Marinelli, and J. B. Rosenzweig, Phys. Rev. Lett. **106**, 164803 (2011).
[17] E. Hemsing, A. Knyazik, F. O'Shea, A. Marinelli, P. Musumeci, et al., Applied Physics Letters **100**, 091110 (pages 4) (2012).
[18] A. Lumpkin and e. al, Proceedings of PAC 2009 pp. 3546–3548. (2009).
[19] C. Behrens et al., Phys. Rev. ST Accel. Beams **15**, 062801 (2012).
[20] E. Saldin, E. Schneidmiller, and M. Yurkov, Nucl. Instrum. Methods Phys. Res., Sect. A **539**, 499 (2005), ISSN 0168-9002.
[21] G. Geloni, P. Ilinski, E. Saldin, E. Schneidmiller, and M. Yurkhov, arXiv:0905.1619 [physics.optics] p. (2009).
[22] R. Bonifacio, C. Pellegrini, and L. Narducci, Optics Communications **50**, 373 (1984).
[23] Y. Shibata, K. Ishi, T. Takahashi, T. Kanai, F. Arai, et al., et al., Phys. Rev. E **49**, 785 (1994).
[24] J. Miao, D. Sayre, and H. N. Chapman, J. Opt. Soc. Am. A **15**, 1662 (1998).
[25] J. R. Fienup, Appl. Opt. **21**, 2758 (1982).
[26] J. Miao, P. Charalambous, J. Kirz, and D. Sayre, Nature. **400**, 342 (1999).
[27] D. Xiang, E. Colby, M. Dunning, S. Gilevich, C. Hast, et al., Phys. Rev. Lett. **105**, 114801 (2010).
[28] D. Xiang, E. Colby, M. Dunning, S. Gilevich, C. Hast, et al., Phys. Rev. Lett. **108**, 024802 (2012).